NASA TECHNICAL MEMORANDUM

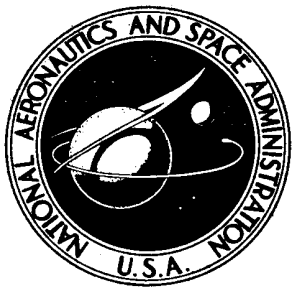

UB
NASA TM X-1921

FLIGHT-MEASURED HEAT TRANSFER AND SKIN FRICTION AT A MACH NUMBER OF 5.25 AND AT LOW WALL TEMPERATURES

by Robert D. Quinn and Frank V. Olinger

Flight Research Center
Edwards, Calif.

NATIONAL AERONAUTICS AND SPACE ADMINISTRATION • WASHINGTON, D. C. • NOVEMBER 1969

1. Report No. NASA TM X-1921	2. Government Accession No.	3. Recipient's Catalog No.
4. Title and Subtitle FLIGHT-MEASURED HEAT TRANSFER AND SKIN FRICTION AT A MACH NUMBER OF 5.25 AND AT LOW WALL TEMPERATURES (U)		5. Report Date November 1969 6. Performing Organization Code
7. Author(s) Robert D. Quinn and Frank V. Olinger		8. Performing Organization Report No. H-579 10. Work Unit No. 722-51-00-01-24
9. Performing Organization Name and Address NASA Flight Research Center P.O. Box 273 Edwards, California 93523		11. Contract or Grant No. 13. Type of Report and Period Covered Technical Memorandum
12. Sponsoring Agency Name and Address National Aeronautics and Space Administration Washington, D. C. 20546		14. Sponsoring Agency Code
15. Supplementary Notes		

16. Abstract (U)

Turbulent skin-friction and heat-transfer coefficients were measured simultaneously on a test panel installed on the sharp-leading-edge upper vertical tail of the X-15 airplane at wall-to-recovery temperature ratios of 0.218 to 0.333 and at a nominal free-stream Reynolds number of 1.54×10^6 per foot (5.05×10^6 per meter). The data were obtained from one flight at a nominal free-stream Mach number of 5.25. Reynolds analogy factors were derived from skin-friction and heat-transfer measurements. The measured data are compared with values predicted by various theories.

17. Key Words Suggested by Author(s)	18. Distribution Statement
Heat transfer - Skin friction - X-15 airplane	U. S. Government and Their Contractors only

19. Security Classif. (of this report)	20. Security Classif. (of this page)	21. No. of Pages	22. Price
Confidential - Group 4	Unclassified	27	

GROUP 4
Downgraded at 3 year intervals;
declassified after 12 years

FLIGHT-MEASURED HEAT TRANSFER AND SKIN FRICTION AT A MACH NUMBER OF 5.25 AND AT LOW WALL TEMPERATURES*

By Robert D. Quinn and Frank V. Olinger
Flight Research Center

SUMMARY

Skin temperatures, shearing forces, and surface static pressures were measured simultaneously on a test panel installed on the sharp-leading-edge upper vertical tail of the X-15 airplane. The data were obtained at a nominal free-stream Mach number of 5.25 and wall-to-recovery temperature ratios of 0.218 to 0.333. The free-stream Reynolds number had a nominal value of 1.54×10^6 per foot (5.05×10^6 per meter). Turbulent heat-transfer coefficients and turbulent skin-friction coefficients were derived from skin-temperature time histories and shear-force measurements, respectively. Also, Reynolds analogy factors were obtained from the measured heat-transfer coefficients and the shearing-stress measurements.

Skin-friction coefficients calculated by the theory of van Driest, Eckert's reference enthalpy method, the Spalding and Chi method, and the adiabatic reference enthalpy method were compared with experimentally determined values. The skin-friction coefficients predicted by the Spalding and Chi method were in excellent agreement with the measured data. The experimental Reynolds analogy factors were compared with values predicted by the methods of Rubesin, von Kármán, and Colburn. The experimentally obtained value of 1.4 was 14 percent to 25 percent higher than the calculated values. Heat-transfer coefficients calculated by using a modified Reynolds analogy between skin friction and heat transfer were compared with measured values. The Spalding and Chi method together with a Reynolds analogy factor of 1.4 predicted heat-transfer coefficients that were in excellent agreement with the measured data. However, when a more commonly used Reynolds analogy factor of 1.2 was applied, values predicted by the theory of van Driest agreed best with the heat-transfer data.

INTRODUCTION

The importance of being able to predict turbulent skin friction and heat transfer for the design of missiles and hypersonic and supersonic vehicles is well known. A large number of empirical and semiempirical theories are available which can be used to predict skin friction and heat transfer at high Mach numbers and low wall temperature ratios. However, values predicted by the various theories usually differ substantially, and, therefore, recourse to experiments must be made to determine the validity of the theories. Unfortunately, data obtained from experiments have also differed. Further,

*Title, Unclassified.

most of the experiments have been performed in wind tunnels, making it necessary to extrapolate to flight conditions.

The X-15 airplane offered a unique opportunity to measure heat transfer and skin friction under quasi-steady flight conditions at high Mach numbers and low wall-to-recovery temperature ratios and thus allow a direct comparison between measured flight data and calculated values. A considerable amount of heat-transfer data (refs. 1 to 6) and some skin-friction data (refs. 6 and 7) were obtained during the X-15 program. The results from these X-15 measurements indicated that the level and rate of change of turbulent skin friction and heat transfer with respect to ratios of wall-to-recovery temperature were lower than predicted by the most widely used theories (for example, Eckert's reference enthalpy (ref. 8) and the theory of van Driest (ref. 9)). However, comparisons of the X-15 data with theory were not conclusive because of the uncertainties of the boundary-layer-edge conditions (as a result of nonuniform flow) and conduction losses. Recent wind-tunnel results reported in reference 10 tended to confirm the X-15 flight results. However, other recent skin-friction and heat-transfer measurements (refs. 11 and 12) are not in agreement with the X-15 data. Furthermore, it has not been established (ref. 13) whether the differences between measured and calculated heat transfer are due to deficiencies in the skin-friction theories or to the use of improper forms of the Reynolds analogy factor, or both.

The present investigation was undertaken to determine the level of turbulent skin friction, heat transfer, and Reynolds analogy factor at very low wall-to-recovery temperature ratios. Consequently, skin friction and heat transfer were measured simultaneously on a constant-pressure (uniform flow field) surface, and Reynolds analogy factors were derived from these measurements. The results of this investigation and comparisons with prediction methods are presented in this paper.

SYMBOLS

The units used for physical quantities in this paper are given both in U.S. Customary Units and the International System of Units (SI). Factors relating the two systems are presented in reference 14; those used in this paper are presented in appendix A.

A — area of skin-friction-gage floating element, 7.629×10^{-4} ft^2 (7.0873×10^{-5} m^2)

C_f — local skin-friction coefficient

$C_{f,i}$ — local incompressible skin-friction coefficient

$c_{p,w}$ — specific heat of skin material, $\frac{\text{Btu}}{\text{lbm-°R}}$ $\left(\frac{\text{J}}{\text{kg-°K}}\right)$

F	shearing force measured by skin-friction gage, lb (hN)
g	gravitational conversion factor, $32.17 \frac{\text{lbm-ft}}{\text{lb-sec}^2}$
H	enthalpy, $\frac{\text{Btu}}{\text{lbm}} \left(\frac{\text{J}}{\text{kg}}\right)$
H_R	boundary-layer-recovery enthalpy, $\frac{\text{Btu}}{\text{lbm}} \left(\frac{\text{J}}{\text{kg}}\right)$
h	geometric altitude, ft (m)
h_H	local heat-transfer coefficient based on enthalpy, $\frac{\text{lbm}}{\text{ft}^2\text{-sec}} \left(\frac{\text{kg}}{\text{m}^2\text{-sec}}\right)$
J	mechanical equivalent of heat, $778 \frac{\text{ft-lb}}{\text{Btu}}$
K	radiation geometry factor, 1.0
M	Mach number
N_{Re}	unit Reynolds number per foot (meter), $\frac{\rho V}{\mu}$
$N_{Re,k}$	local Reynolds number, $\frac{\rho_l V_l x_k}{\mu_l}$
N_{St}	local Stanton number, $\frac{h_H}{\rho_l V_l}$
$N_{St,i}$	local incompressible Stanton number
P	total pressure, $\frac{\text{lb}}{\text{ft}^2} \left(\frac{\text{hN}}{\text{m}^2}\right)$
p	absolute static pressure, $\frac{\text{lb}}{\text{ft}^2} \left(\frac{\text{hN}}{\text{m}^2}\right)$

q	dynamic pressure, $\frac{lb}{ft^2}\left(\frac{hN}{m^2}\right)$
s	Reynolds analogy factor (see eq. (6))
T	temperature, °R (°K)
T_R	boundary-layer-recovery temperature, °R (°K)
t	time, sec
V	velocity, $\frac{ft}{sec}\ \left(\frac{m}{sec}\right)$
x	distance from leading edge, ft (m)
x_k	flow length measured chordwise from boundary-layer trips to midway between skin-friction gage and thermocouples, 2.52 ft (0.767 m)
$\delta_{v,eff}$	vertical-tail deflection with respect to free-stream flow direction, deg
δ_w	skin thickness, 0.0605 in. ±0.001 (0.1537 cm ±0.00254)
ϵ	emissivity of test surface, 0.76
η	recovery factor, 0.9
μ	dynamic viscosity, $\frac{lbm}{ft\text{-}sec}\ \left(\frac{N\text{-}sec}{m^2}\right)$
ρ	density of air, $\frac{lbm}{ft^3}\left(\frac{kg}{m^3}\right)$
ρ_w	density of skin material, $515\ \frac{lbm}{ft^3}\ \left(8250\ \frac{kg}{m^3}\right)$
σ	standard deviation

σ_S	Stefan-Boltzmann constant, 4.78×10^{-13} $\frac{\text{Btu}}{\text{ft}^2\text{-sec-}^\circ\text{R}^4}$ $\left(5.67 \times 10^{-8} \frac{\text{W}}{\text{m}^2\text{-}^\circ\text{K}^4}\right)$
τ	shearing stress $\frac{F}{A}$, $\frac{\text{lb}}{\text{ft}^2}$ $\left(\frac{\text{hN}}{\text{m}^2}\right)$

Subscripts:

av	average
l	local
w	wall
∞	free stream

DESCRIPTION OF EQUIPMENT

The experimental apparatus was installed on the upper vertical tail of the X-15 number 3 (X-15-3) airplane (fig. 1). A detailed description of the airplane is given in

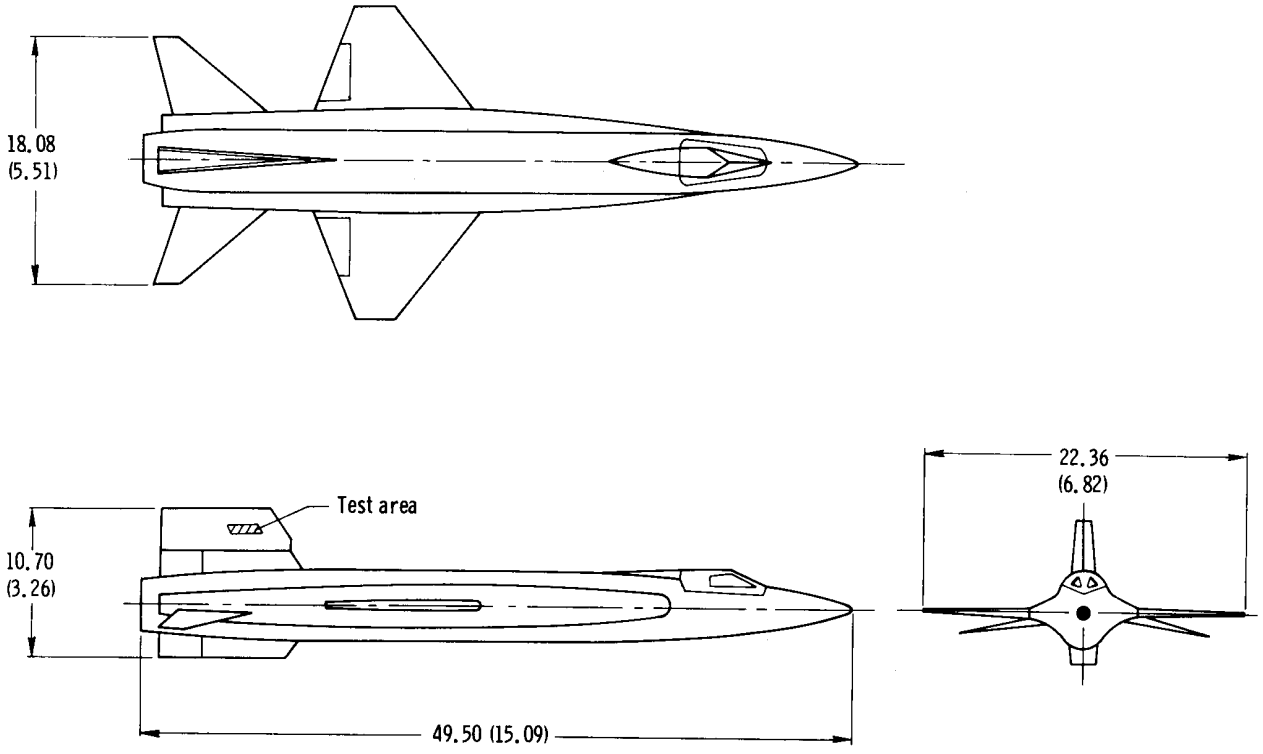

Figure 1.– Sketch of the X-15 airplane. Dimensions in feet (meters).

reference 5. The vertical tail was a 5° half-angle wedge with a 30° swept sharp leading edge. Boundary-layer trips consisting of spot welds 0.125 inch (0.318 centimeter) in diameter, 0.025 inch (0.0635 centimeter) high, and 1.0 inch (2.54 centimeters) apart were installed parallel to and 4.8 inches (12.19 centimeters) aft of the leading edge (fig. 2).

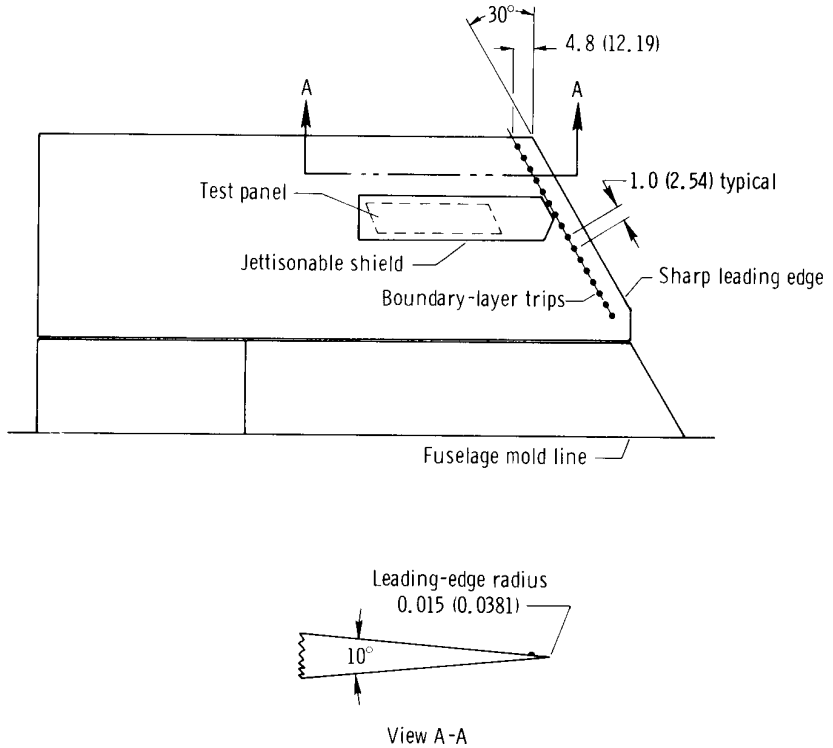

Figure 2.-- Sketch of upper vertical tail showing boundary-layer trips, test panel, and jettisonable shield locations. All dimensions in inches (centimeters) unless otherwise noted.

The test panel was constructed of Inconel-X and was 0.0605 inch ±0.001 (0.1537 centimeter ±0.00254) thick. The panel was designed to maintain a flat surface during the test and was installed on the right side (pilot's right) of the vertical tail at the approximate location shown in figure 2. A photograph of the test panel installed on the vertical tail is shown in figure 3(a). To provide access to the instrumentation, a removable panel was installed on the left side (directly opposite the test panel) of the vertical tail.

To obtain the desired wall-to-recovery temperature ratios and to assure an isothermal test surface when the airplane reached the desired speed and altitude, it was necessary to insulate the test panel during the initial phase of the flight profile. Consequently, an insulating cover was installed over the test area as shown in figure 2. A photograph of the jettisonable shield installed on the vertical tail is shown in figure 3(b). At a predetermined speed and altitude the cover was jettisoned, instantaneously (50 milliseconds) exposing the test surface to the airstream, at which time data were obtained.

Since the panel opposite the test panel (access panel) was exposed to aerodynamic heating during the entire portion of the flight, a radiation shield was placed between the test panel and the access panel to insulate the test panel and instrumentation from internal radiation.

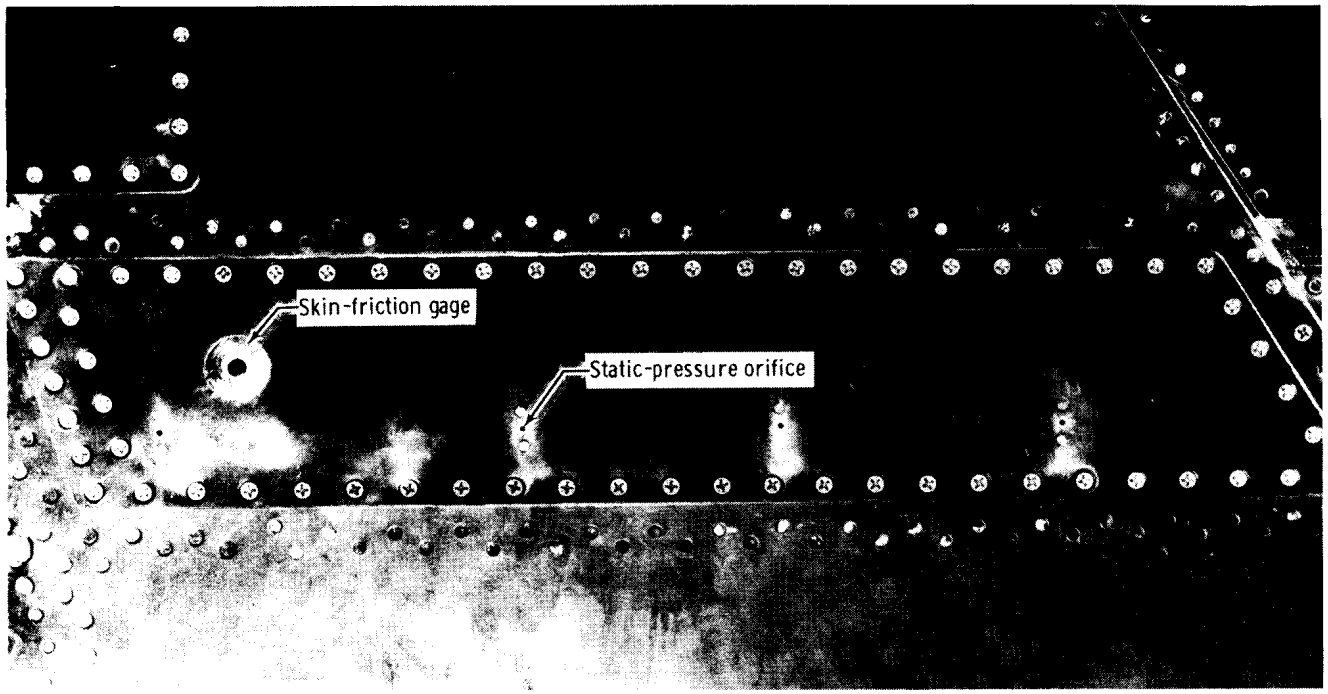

(a) Test panel installed on vertical tail.

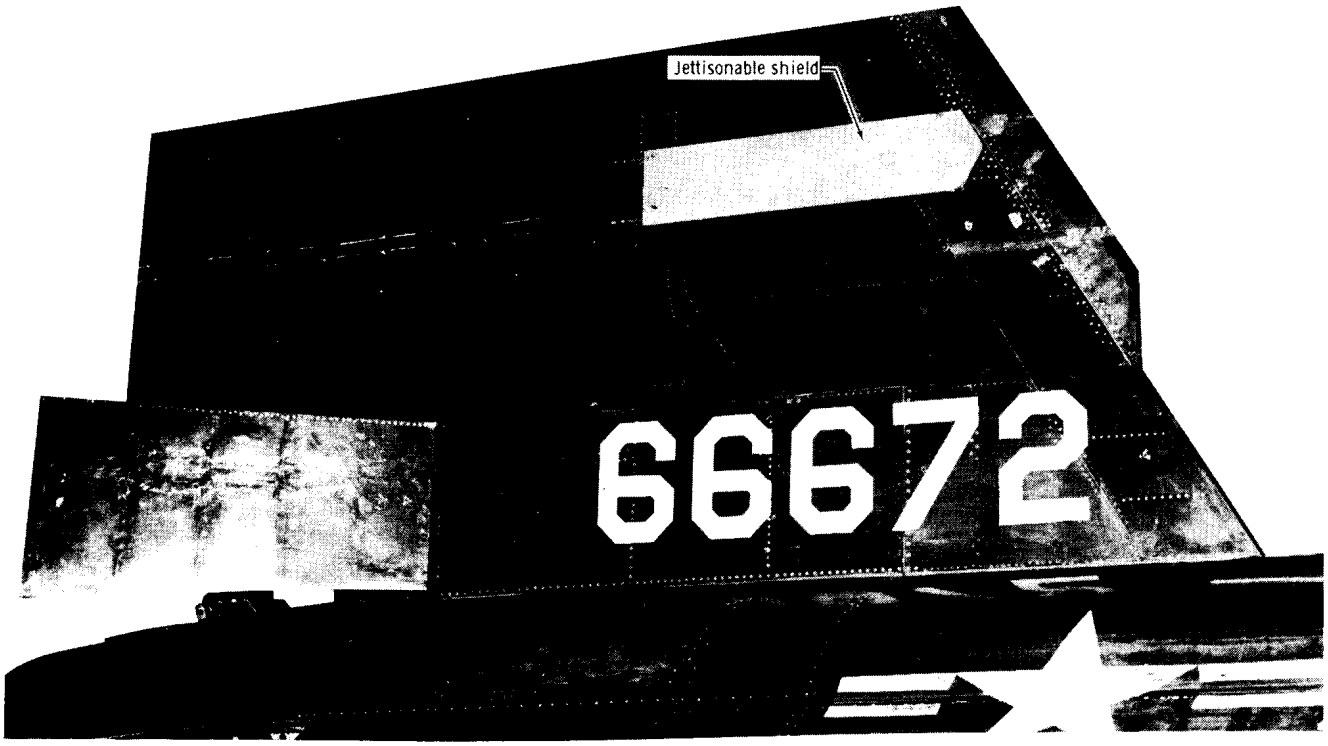

(b) Jettisonable shield installed on vertical tail.

Figure 3.– Photograph of vertical tail showing test panel and jettisonable shield.

INSTRUMENTATION

The test panel was instrumented with thermocouples, static-pressure orifices, and a skin-friction gage as shown in figure 4. Outputs from the thermocouples, pressure transducers, and skin-friction gage were recorded on tape by a pulse code modulation (PCM) data-acquisition system at a rate of 50 samples per second. The accuracy of the PCM system was ±0.3 percent of full scale. The individual instruments are discussed in the following sections.

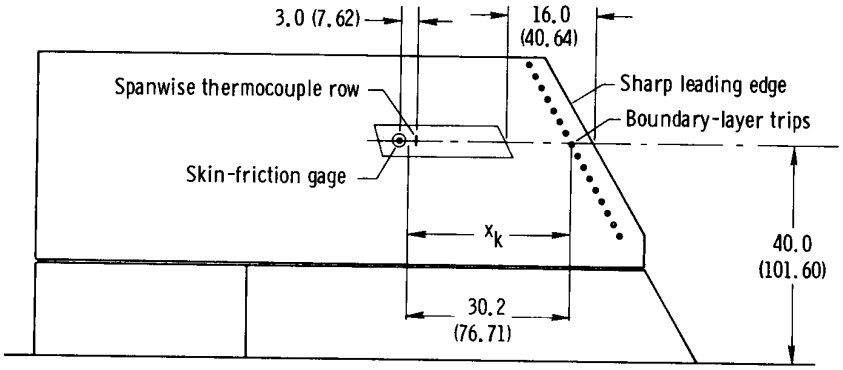

(a) Location of test panel and instrumentation.

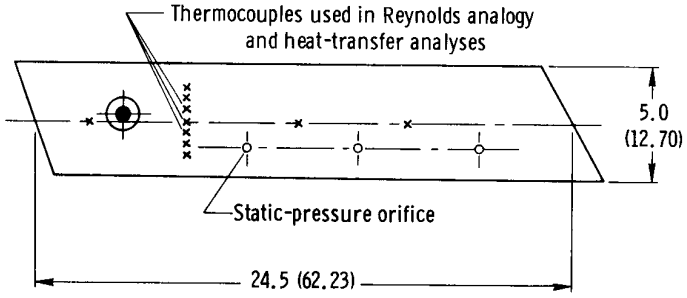

(b) Instrumented test panel.

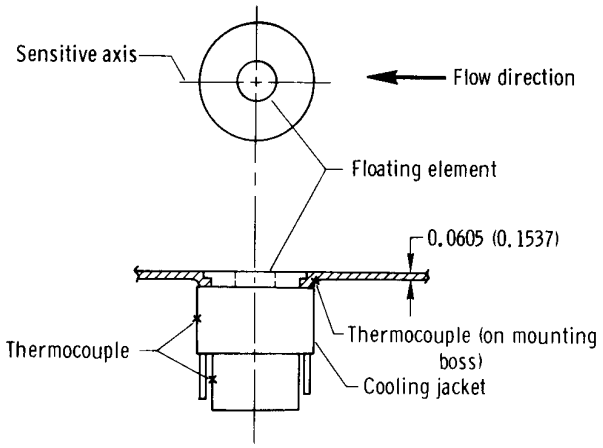

(c) Skin-friction-gage installation.

Figure 4.-- Location and installation of instrumentation. Dimensions in inches (centimeters).

Skin-Friction Gage

The skin-friction gage used in this experiment was a commercially developed liquid-cooled force balance. The floating element (fig. 4(c)) was kept centered by electromagnets, and any force attempting to displace the floating element along its sensitive axis was countered by an increase in voltage to the electromagnets. The voltage necessary to keep the element centered was recorded and converted to shearing force by an appropriate calibration. The floating element did not protrude above and was less than 0.0005 inch (0.00127 centimeter) below the surface of the gage body at room temperature. The space between the floating element and gage body was uniform and less than 0.001 inch (0.00254 centimeter) with power applied to the gage. Detailed descriptions of the skin-friction balance and the cooling system used to keep the balance within design limits are given in reference 7.

To obtain a good measurement of the shearing stress the skin-friction balance must be mounted with its sensitive axis parallel to the flow direction. Motion pictures obtained from an oil-flow study of the surface flow on a 1/50-scale model of the X-15 airplane at the NASA Langley Research Center showed that, for the angle of attack (approximately 3°) of this experiment, the flow was in the chordwise direction (parallel to the centerline of the aircraft). The skin-friction gage was mounted accordingly (fig. 4(c)). The exposed surface (surface exposed to the airstream) of the gage was mounted flush (within ±0.0001 inch (±0.000254 centimeter)) with the exposed surface of the test panel, and the space between the gage and the test panel was less than 0.0001 inch (0.000254 centimeter). As shown in figure 4(c), thermocouples were installed on the gage body, cooling jacket, and panel boss directly beneath the edge of the exposed surface of the gage. The thermocouples on the gage body and cooling jacket were used to determine if the cooling system was operating and that the temperature of the gage body stayed within design limits. The thermocouple on the boss was installed to measure a temperature as near the exposed surface of the gage as possible.

Thermocouples

Ten 22-gage chromel-alumel thermocouples were spot-welded to the inner surface of the test panel at the locations shown in figure 4(b). Seven thermocouples were installed spanwise at 0.5-inch (1.27-centimeter) intervals and 3 inches (7.62 centimeters) in front of the skin-friction gage. These thermocouples were installed in this manner to detect any spanwise conduction losses. The other thermocouples fore and aft of the skin-friction gage were used to check the uniformity of the chordwise temperature distribution.

Pressure Orifices

Three surface static-pressure orifices were installed flush with the surface of the test panel at the locations shown in figure 4(b). The pressure orifices had an inside diameter of 0.125 inch (0.318 centimeter) and were connected to transducers mounted directly behind the test panel. Thermocouples were installed on the transducers to determine if their temperatures stayed within design limits.

DATA REDUCTION

The shearing force measured by the skin-friction gage was reduced to the shearing stress by using the following equation:

$$\tau = \frac{F}{A} \tag{1}$$

where A is 7.629×10^{-4} ft^2 (7.0873×10^{-5} m^2) and is the area of the floating element of the skin-friction gage.

The shearing stress was reduced to the skin-friction coefficient by using the equation

$$C_f = \frac{2\tau g}{\rho_l V_l^2} \tag{2}$$

where the local density ρ_l and the local velocity V_l were computed from the measured static pressure together with the calculated total pressure behind the leading-edge oblique shock wave. The total pressure behind the leading-edge shock was computed assuming free-stream conditions in front of the vertical tail and neglecting the sweep angle (ref. 3).

The measured heat-transfer coefficients were obtained from the following thin-skin heating equation (ref. 4):

$$h_H = \frac{\rho_w c_{p,w} \delta_w \frac{dT_w}{dt} + \sigma_S \epsilon K T_w^4}{(H_R - H_w)} \tag{3}$$

This equation neglects internal radiation and conduction losses. A radiation shield was installed behind the test panel; therefore, radiation losses were negligible. Data from the thermocouples on the test panel showed that there were no conduction losses during the test.

The experimental Stanton number was determined by using the following relationship:

$$N_{St} = \frac{h_H}{\rho_l V_l} \tag{4}$$

Assuming that total enthalpy is constant, the recovery enthalpy may be computed from the relationship

$$H_R = H_\infty + \frac{V_\infty^2 - V_l^2}{2gJ} + \eta \frac{V_l^2}{2gJ} \tag{5}$$

where

$$H_\infty = f(T_\infty, p_\infty) \text{ (ref. 15)}$$

$$H_W = f(T_W, p_l) \text{ (ref. 15)}$$

$$\eta = 0.9$$

The skin heating rates $\frac{dT_W}{dt}$ were graphically determined by making plots of wall temperature versus time, fairing a curve through the data, and determining the slopes by means of a front-surfaced mirror. Skin heating rates were determined in this manner for data obtained from the three thermocouples near the center of the panel and 3 inches in front of the skin-friction gage. (See fig. 4(b).) Therefore, three values of the skin heating rates were obtained for each time at which heat-transfer coefficients were derived. These values agreed within ±1 R deg/sec (±0.556 K deg/sec). The average of these three values was used in equation (3) to obtain the measured heat-transfer coefficient.

The density ρ_W of Inconel-X is a constant 515 lbm/ft^3 (8250 kg/m^3). The specific heat $c_{p,w}$ was obtained from reference 16 and varied from 0.102 $\frac{\text{Btu}}{\text{lbm-°R}}$ $\left(4.26 \times 10^2 \frac{\text{J}}{\text{kg-°K}}\right)$ to 0.113 $\frac{\text{Btu}}{\text{lbm-°R}}$ $\left(4.72 \times 10^2 \frac{\text{J}}{\text{kg-°K}}\right)$ for the test conditions of this experiment. The emissivity ϵ of the test surface had a nominal value of 0.76 (ref. 17), and the skin thickness δ_W of the test panel was 0.0605 inch ±0.001 (0.1537 centimeter ±0.00254).

Heat transfer can be related to skin friction by a Reynolds analogy factor as follows:

$$N_{St} = s\frac{C_f}{2}$$

or

$$\frac{h_H}{\rho_l V_l} = s\frac{\tau g}{\rho_l V_l^2}$$

Therefore

$$s = \frac{2N_{St}}{C_f} = \frac{h_H V_l}{\tau g} \tag{6}$$

where h_H and τ are the measured heat-transfer coefficient and shearing stress, respectively, and V_l is the calculated local velocity.

Equation (6) was used to obtain the experimental Reynolds analogy factor.

ACCURACY

The accuracy of the measured skin friction, heat transfer, and Reynolds analogy factor is analyzed in appendix B. The results of this analysis are summarized in the following tabulation:

$\frac{\sigma_\tau}{\tau}$	±4 percent
$\frac{\sigma_{C_f}}{C_f}$	±9.3 percent
$\frac{\sigma_{h_H}}{h_H}$	±5.1 percent
$\frac{\sigma_{N_{St}}}{N_{St}}$	±9.1 percent
$\frac{\sigma_s}{s}$	±6.8 percent

TEST CONDITIONS

The X-15-3 airplane was launched from a B-52 carrier aircraft at 45,000 feet (13,700 meters) altitude, climbed under power to the desired speed and altitude, was throttled back and maintained at near-constant flight conditions until burnout, and then glided to a landing at Edwards Air Force Base, Calif. When the specified speed and altitude were reached and quasi-steady conditions obtained, the insulating cover over the test panel was jettisoned and data were obtained during the 10-second period prior to fuel depletion.

Time histories of free-stream Mach number, free-stream dynamic pressure, and altitude are shown in figure 5. The shaded portion of the flight profiles indicates the quasi-steady period after the shield was jettisoned during which the data were obtained. All pertinent flight parameters for this period are listed in table I. The measured wall temperatures, shearing stresses, heat-transfer coefficients, and surface static pressures together with other pertinent calculated local flow parameters are listed in table II. Heat-transfer and skin-friction coefficients were derived at free-stream Mach numbers of 5.19 to 5.33, free-stream Reynolds numbers of 1.57×10^6 per foot (5.15×10^6 per meter) to 1.51×10^6 per foot (4.95×10^6 per meter) and wall-to-recovery temperature ratios of 0.218 to 0.333.

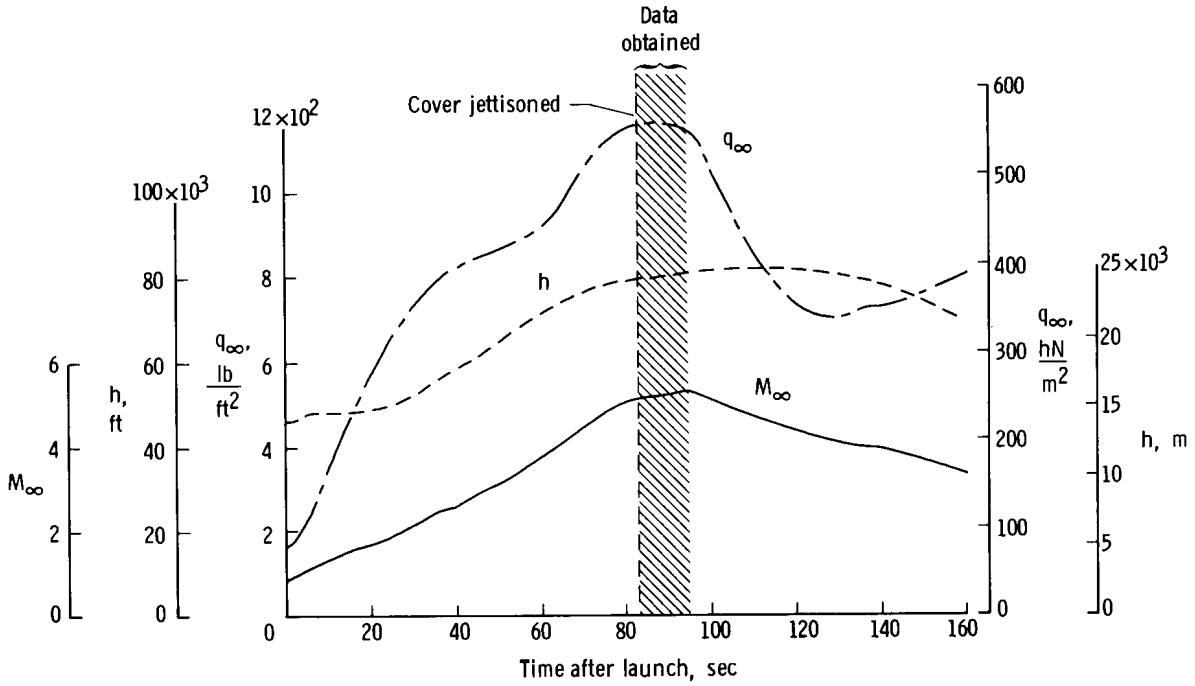

Figure 5.– Time history of flight parameters.

RESULTS AND DISCUSSION

Local Flow Conditions

Surface static pressures were measured at three locations on the test panel (fig. 4(b)). An average value of the three measured static pressures was determined for each time at which heat-transfer coefficients were derived. These average values were used in the data analyses and are tabulated in table II. The other pertinent local flow parameters were computed from the average measured static pressures together with the calculated total pressure behind the oblique shock wave. The total pressure was computed by the procedure discussed in the DATA REDUCTION section. The flow length x_k used to compute the local Reynolds numbers tabulated in table II had a value of 2.52 feet (0.767 meter) and was measured from the boundary-layer trips[1] to midway between the spanwise row of thermocouples and the skin-friction gage (fig. 4(a)).

Skin Friction

The experimental skin-friction coefficients divided by the calculated incompressible skin-friction coefficients are plotted in figure 6(a) versus ratios of wall-to-recovery temperature. The incompressible skin-friction coefficients were computed by the

[1]The virtual origin of the turbulent boundary layer was assumed to be at the boundary-layer trips. The possibility that the virtual origin may have been located aft of the trips is discussed in appendix C.

Kármán-Schoenherr skin-friction equation (ref. 18). The measured data show practically nc variation with change in temperature ratio for the limited range of wall temperatures covered in this experiment and are in fair agreement with previous measurements obtained on the X-15 airplane (ref. 7). Also shown in figure 6(a), for comparison, are skin-friction values predicted by the theory of van Driest (ref. 9), the Spalding and Chi method (ref. 19), the reference enthalpy method (ref. 8), and the adiabatic reference enthalpy method (ref. 4). The values calculated by using the theory of van Driest and the reference enthalpy method are 12 percent to 24 percent higher than the measured data, whereas values calculated by using the adiabatic reference enthalpy method are approximately 24 percent lower than the measured data. However, the values predicted by the Spalding and Chi method are in excellent agreement with the measured skin-friction coefficients.

The effect of a possible step temperature at the skin-friction balance was considered in the analysis of the data. Temperatures obtained from the thermocouples along the length of the test panel showed that the surface was isothermal during the test. However, it was not possible to measure directly the temperature of the exposed surface of the gage. In an attempt to estimate the temperature of the exposed surface, a thermocouple was placed on the boss just beneath the edge of the surface of the gage (fig. 4(c)). The temperature of the boss is believed to be a reasonable approximation of the surface temperature of the gage because the boss is in direct contact with the cooling jacket and, therefore, has a high rate of conduction loss which tends to compensate for the high heat-storage capacity of the skin-friction gage. A temperature difference between the boss and the test surface of 50 R° (27.8 K°) was measured 5 seconds after the shield was jettisoned. Five seconds later, the temperature difference was 100 R° (55.6 K°). A step temperature of 50 R° (27.8 K°) would have a negligible effect on the measurements (ref. 20). Therefore, the initial five data points in figure 6(a) are considered to be free from any appreciable step-temperature effects. Whether or not a step temperature of 100 R° (55.6 K°) would significantly affect the data is questionable. However, the measured heat-transfer coefficients (discussed in a subsequent section) which were not subjected to any temperature discontinuity show essentially the same variation with wall temperature as do the skin-friction measurements. Since it is reasonable to expect the skin friction and heat transfer to have the same variation with wall temperature, it would appear that the temperature discontinuity that did exist during the test at the skin-friction gage was not sufficient to have any discernible effect on the shearing-force measurements.

Reynolds Analogy Factor

Most turbulent heat-transfer methods are based on some form of Reynolds analogy between skin friction and heat transfer. Consequently, once a skin-friction equation is selected, a Reynolds analogy factor is needed in order to calculate a heat-transfer coefficient. The determination of a Reynolds analogy factor has been the subject of considerable investigation but has still not been resolved (refs. 6 and 11 to 13).

Comparisons between experimental and calculated Reynolds analogy factors are shown in figure 6(b). The experimental Reynolds analogy factors were derived from measured heat-transfer coefficients, measured shearing stresses, and calculated local velocities by using equation (6). The theoretical values are those most commonly used in heat-transfer analyses and were calculated by the methods of Rubesin (ref. 21), Kármán (ref. 22), and Colburn (ref. 23). The Kármán and Colburn forms of the

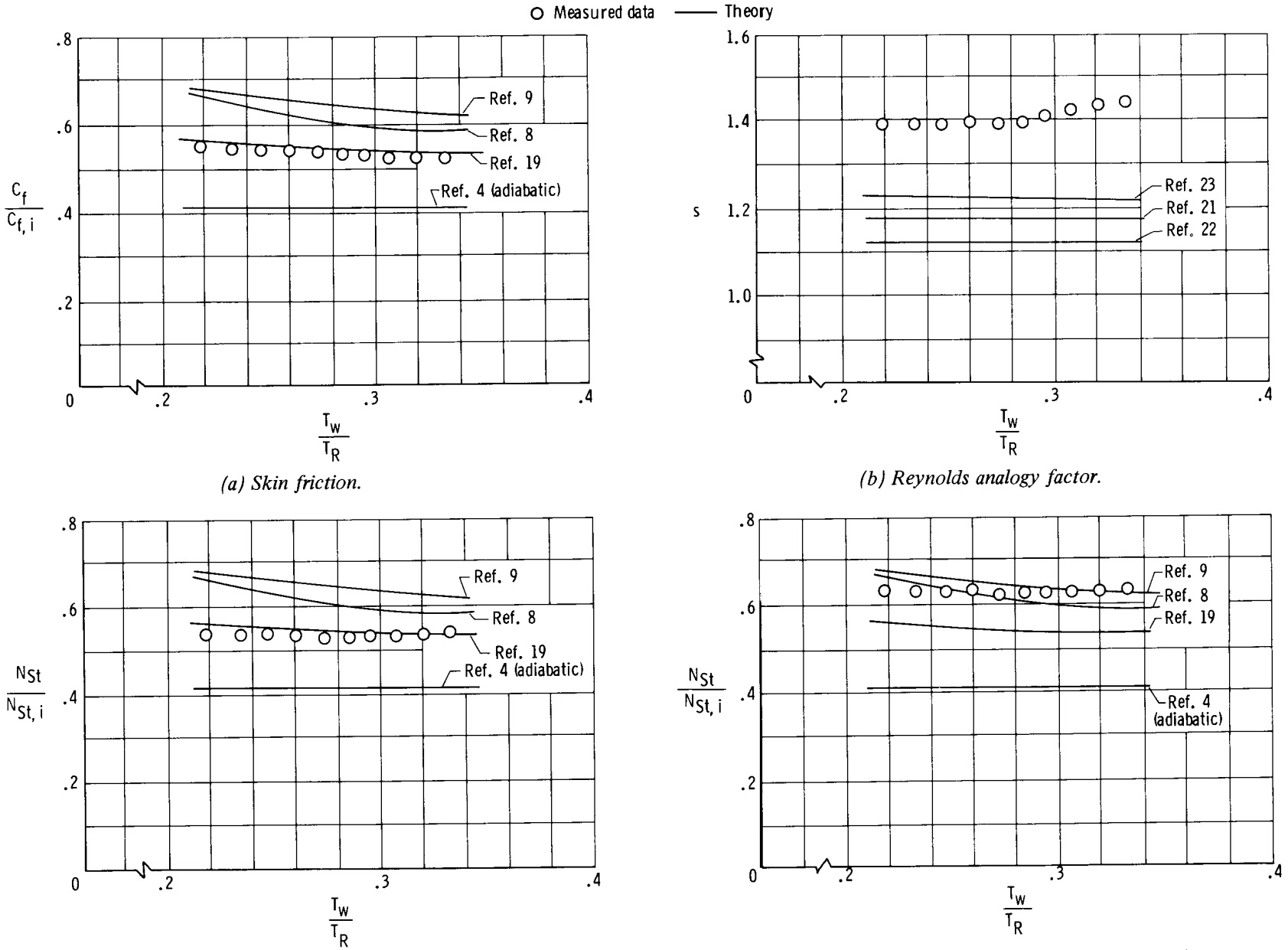

(a) Skin friction.

(b) Reynolds analogy factor.

(c) Heat transfer (Reynolds analogy factor = 1.4).

(d) Heat transfer (Reynolds analogy factor = 1.2).

Figure 6.– Comparison of measured and calculated skin friction, Reynolds analogy factor, and heat transfer.

Reynolds analogy factor were extended to compressible flow as explained in references 13 and 8, respectively. As shown, the experimental Reynolds analogy factor has a value of approximately 1.4, which is 14 percent to 25 percent higher than the calculated values. The variation of the measured data with the ratio of wall-to-recovery temperature shown in figure 6(b) is not considered significant, since it is within the accuracy of the measurements.

Heat Transfer

Experimentally determined Stanton numbers divided by calculated incompressible Stanton numbers are plotted versus wall-to-recovery temperature ratios in figures 6(c) and 6(d). The incompressible Stanton numbers were computed from the Kármán-Schoenherr flow equation (ref. 18) by using a modified Reynolds analogy between skin friction and heat transfer. As can be seen, the measured heat transfer shows essentially the same variation with temperature ratio as obtained for the skin-friction measurements. Also shown in figures 6(c) and 6(d) are the normalized Stanton numbers predicted by the skin-friction theories of van Driest (ref. 9), Spalding and Chi (ref. 19), Eckert's reference enthalpy (ref. 8), and the adiabatic reference enthalpy (ref. 4) using Reynolds analogy factors of 1.4 and 1.2 for both the compressible and incompressible calculated Stanton numbers. Figure 6(c) shows the values obtained from these theories by using the experimentally determined Reynolds analogy factor of 1.4. As can be seen, values predicted by the Spalding and Chi method are in excellent agreement with the measured data, whereas values calculated by using the theory of van Driest and Eckert's reference enthalpy method are 9 to 25 percent higher than the measured data.

Although this experiment showed the Reynolds analogy factor to have a value of approximately 1.4, it is of interest to know how the various theories would compare with the measured data if a more generally accepted value of the Reynolds analogy factor were used. Consequently, the calculated values were compared with the experimentally determined Stanton numbers, assuming a Reynolds analogy factor of 1.2. These comparisons are presented in figure 6(d). As shown, the values predicted by the theory of van Driest and Eckert's reference enthalpy method are in fair agreement with the measured data. This result is not in agreement with previous X-15 heat-transfer results (for example, ref. 4) which showed the data to be 20 to 30 percent lower than the values predicted by the theory of van Driest and the reference enthalpy method. There are several possible reasons why the present heat-transfer measurements are higher than the previous X-15 results. First, the previous measurements (refs. 1 to 4) were compared with theory using the Blasius resistance formula, whereas the present analysis utilized the Kármán-Schoenherr equation. For the conditions of this test, the use of the Blasius formula would decrease the normalized measured Stanton numbers $\left(\frac{N_{St}}{N_{St,i}}\right)$ by 7 percent. Second, most of the previous data were measured on surfaces with blunt leading edges, which made it difficult to establish the boundary-layer-edge conditions. Third, conduction and internal radiation losses were known more accurately for the present test; and, fourth, the present data were obtained at lower ratios of wall-to-recovery temperature than the previous data.

CONCLUSIONS

An investigation of the turbulent boundary layer on a constant-pressure surface at a Mach number of 5.25 and at low wall-to-recovery temperature ratios led to the following conclusions:

1. The skin-friction coefficients predicted by the Spalding and Chi method were in excellent agreement with the measured data, whereas values predicted by the theory of van Driest and Eckert's reference enthalpy method were higher than the measured data.

2. The experimentally determined Reynolds analogy factor of 1.4 was 14 percent to 25 percent higher than the theoretically predicted values.

3. Stanton numbers calculated by using the Spalding and Chi theory were also in excellent agreement with the measured data when the experimental Reynolds analogy factor of 1.4 was used. However, when a Reynolds analogy factor of 1.2 was used, values predicted by the theory of van Driest agreed best with the heat-transfer measurements.

Flight Research Center,
National Aeronautics and Space Administration,
Edwards, Calif., August 19, 1969.

APPENDIX A

CONVERSION OF U.S. CUSTOMARY UNITS TO SI UNITS

The International System of Units (SI) was adopted by the Eleventh General Conference on Weights and Measures, Paris, October 1960, in Resolution No. 12 (ref. 14). Conversion factors for the units used herein are given in the following table:

Physical quantity	U.S. Customary Unit	Conversion factor [1]	SI Unit
Area	ft^2	0.0929	m^2
Density	lbm/ft^3	16.02	kg/m^3
Dynamic viscosity	lbm/ft-sec	1.488	$N\text{-}sec/m^2$
Enthalpy	Btu/lbm	2.32×10^3	J/kg
Shearing force	lb	4.448×10^{-2}	hN
Shearing stress, Pressure	lb/ft^2	0.4788	hN/m^2
Heat-transfer coefficient	$lbm/ft^2\text{-}sec$	4.883	$kg/m^2\text{-}sec$
Length	ft	0.3048	m
	in.	2.54	cm
Specific heat	Btu/lbm-°R	4.18×10^3	J/kg-°K
Temperature	°R	0.556	°K
Velocity	ft/sec	0.3048	m/sec

[1] Multiply value given in U.S. Customary Unit by conversion factor to obtain equivalent value in SI Unit.

Prefixes to indicate multiple units are:

Prefix	Multiple
milli (m)	10^{-3}
centi (c)	10^{-2}
hecto (h)	10^2
kilo (k)	10^3

APPENDIX B

ERROR ANALYSIS

Estimated Errors

The most probable error in the measured data was estimated by using the concept of a limit error. In combination with a Gaussian distribution, the most probable error (ref. 24) is equal to the standard deviation σ and represents the deviation for which the probability of being exceeded is 0.32. The standard deviations σ of the quantities used in this analysis are given in the following table:

Quantity	Limit error (3σ)	Standard deviation (σ)
$\frac{dT_w}{dt}$	±2.0 R°/sec (±1.11 K°/sec)	±0.67 R°/sec (±0.372 K°/sec)
T_w	±12 R° (±6.67 K°)	±4 R° (±2.22 K°)
H_w	----------	±0.97 Btu/lbm (±0.225 kJ/kg)
δ_w	----------	±1.6 percent
T_∞	----------	±1 percent
H_∞	----------	±1 percent
V_∞	----------	±1.4 percent
$c_{p,w}$	----------	±3 percent
M_∞	----------	±1.5 percent
p_∞	----------	±9.3 percent
P_∞	----------	±10 percent
ϵ	----------	±7.4 percent
P_l	----------	±10 percent
p_l	----------	±7 percent
τ	----------	±4 percent
V_l	----------	±2.1 percent
ρ_l	----------	±7.2 percent

The skin heating rates $\frac{dT_w}{dt}$ were graphically determined as described in the DATA REDUCTION section. Numerous determinations of the slopes by the graphical method have shown that the maximum error in the slopes was ±2.0 R°/sec (±1.11 K°/sec). Consequently, this value was taken as the limit error (3σ) for the skin heating rates.

The error in skin thickness was determined from actual measurements of the test panel. The values of σ_{T_∞}, σ_{V_∞}, σ_{M_∞}, σ_{p_∞}, and σ_{P_∞} were obtained from references 25 and 26. The values for σ_{H_w} and σ_{H_∞} were determined by using σ_{T_w} and σ_{T_∞} together with reference 15. The errors in emissivity σ_ϵ, shearing stress σ_τ, and specific heats $\sigma_{c_{p,w}}$ were obtained from references 16, 7, and 27, respectively.

The local static pressure was measured by absolute 0 to 5 psi ($0 \text{ to } 3.45 \times 10^{-6} \frac{N}{cm^2}$) transducers with an accuracy of ±1 percent of full scale. The local total pressure was computed from the total-pressure ratio across an attached oblique shock together with the free-stream total pressure. The total-pressure ratio was assumed to be correct, and, therefore, the local total pressure has the same percentage errors as the free-stream total pressure. The local total-pressure error σ_{P_l} and local static-pressure error σ_{p_l} were used in conjunction with the appropriate isentropic relationships (ref. 28) to obtain σ_{V_l} and σ_{ρ_l}.

Total Errors in C_f, h_H, N_{St}, and s

The logarithmic differentials of equations (2), (3), (4), and (6) were determined, and the fractional standard deviation for each quantity was combined as an independent error (ref. 29) according to the following equations:

$$\left(\frac{\sigma_{C_f}}{C_f}\right)^2 = \left(\frac{\sigma_\tau}{\tau}\right)^2 + \left(\frac{\sigma_{\rho_l}}{\rho_l}\right)^2 + (4)\left(\frac{\sigma_{V_l}}{V_l}\right)^2 \tag{B1}$$

$$\left(\frac{\sigma_{h_H}}{h_H}\right)^2 = \left(\frac{A\frac{dT_w}{dt}}{Z}\right)^2 \left(\frac{\sigma_{\delta_w}}{\delta_w}\right)^2 + \left(\frac{A\frac{dT_w}{dt}}{Z}\right)^2 \left(\frac{\sigma_{c_{p,w}}}{c_{p,w}}\right)^2 + \left(\frac{A\frac{dT_w}{dt}}{Z}\right)^2 \left(\frac{\sigma_{\frac{dT_w}{dt}}}{\frac{dT_w}{dt}}\right)^2$$

$$+ \left(\frac{4\sigma_S \epsilon T_w^4}{Z}\right)^2 \left(\frac{\sigma_{T_w}}{T_w}\right)^2 + \left(\frac{\sigma_S \epsilon T_w^4}{Z}\right)^2 \left(\frac{\sigma_\epsilon}{\epsilon}\right)^2 + \left(\frac{H_w}{H_R - H_w}\right)^2 \left(\frac{\sigma_{H_w}}{H_w}\right)^2$$

$$+ \left(\frac{H_\infty}{H_R - H_w}\right)^2 \left(\frac{\sigma_{H_\infty}}{H_\infty}\right)^2 + \left(\frac{2(H_R - H_\infty)}{H_R - H_w}\right)^2 \left(\frac{\sigma_{V_\infty}}{V_\infty}\right)^2 \tag{B2}$$

where

$$A = \rho_w c_{p,w} \delta_w$$

$$Z = A \frac{dT_w}{d\tau} + \sigma_S \epsilon T_w^4$$

$$H_R = H_l + \eta \frac{V_l^2}{2gJ} \approx H_\infty + 0.9 \frac{V_\infty^2}{2gJ}$$

$$\left(\frac{\sigma_{N_{St}}}{N_{St}}\right)^2 = \left(\frac{\sigma_{h_H}}{h_H}\right)^2 + \left(\frac{\sigma_{\rho_l}}{\rho_l}\right)^2 + \left(\frac{\sigma_{V_l}}{V_l}\right)^2 \tag{B3}$$

$$\left(\frac{\sigma_s}{s}\right)^2 = \left(\frac{\sigma_{h_H}}{h_H}\right)^2 + \left(\frac{\sigma_{V_l}}{V_l}\right)^2 + \left(\frac{\sigma_\tau}{\tau}\right)^2 \tag{B4}$$

By using the preceding equations, errors were computed for each time at which heat-transfer coefficients were derived. The variation in the errors from time 83.8 seconds to 92.8 seconds was insignificant. Consequently, only one error for each quantity is listed in the ACCURACY section.

APPENDIX C

DETERMINATION OF THE VIRTUAL ORIGIN OF THE TURBULENT BOUNDARY LAYER

This experiment was originally designed to be performed at a dynamic pressure of 1600 lb/ft^2 (76.6 hN/m^2). However, because of structural problems with the vertical tail, the dynamic pressure was limited to 1200 lb/ft^2 (57.5 hN/m^2). Because of this lower dynamic pressure and corresponding lower Reynolds number, the effectiveness of the boundary-layer trips was questionable. Consequently, heat-transfer coefficients were computed by using data obtained from the thermocouples shown in figure 7.

The Stanton numbers obtained from these thermocouples are plotted in figure 7 versus distance from the leading edge. As can be seen, data from the most forward thermocouple show that the flow was initially turbulent and gradually changed to transitional. The data from the next thermocouple show some variation with time, but appear to be turbulent. The data from the thermocouples used in the heat-transfer and skin-friction analyses are also turbulent and show no appreciable variation with time. It should be noted that, although the latter data appear to be turbulent, there is not sufficient information to establish definitely that there was fully developed turbulent flow (ref. 30) and that the measurements were not obtained in the region of peak heating that occurs near the end of transition (ref. 13). However, on the basis of the data shown in figure 7, it is probable that the virtual origin is located somewhere between the trips and the first thermocouple on the test panel.

A commonly used point for the virtual origin is the end of laminar flow (ref. 31). To determine the end of laminar flow for the present test, the data presented in figure 7 were used in the following analysis. The data from the second thermocouple station were assumed to be the beginning of fully developed turbulent flow for times 91.8 seconds and 92.8 seconds after launch. A straight line was drawn from the turbulent data through the two transitional points obtained from the forward thermocouple station. The intersection of this line with the laminar theory line (point A) was taken as the end of laminar flow for times 91.8 seconds and 92.8 seconds after launch. For times 83.8 seconds to 90.8 seconds after launch, the beginning of turbulent flow was assumed to be at the forward thermocouple station. A straight line was drawn through the forward turbulent data parallel to the previously drawn line. The intersection of this line with the laminar theory line (point B) is the assumed end of laminar flow for all but the last 2 seconds of data. It may be noted that the length of transition obtained by this procedure is in agreement with the results of reference 31 which, in turn, were in agreement with Cole's work (ref. 32).

The data in figures 6(a), 6(c), and 6(d) are based on a flow length measured from the boundary-layer trips and would change by only approximately 2 percent if the flow length were measured from the location represented by point B in figure 7. Consequently, no corrections were made.

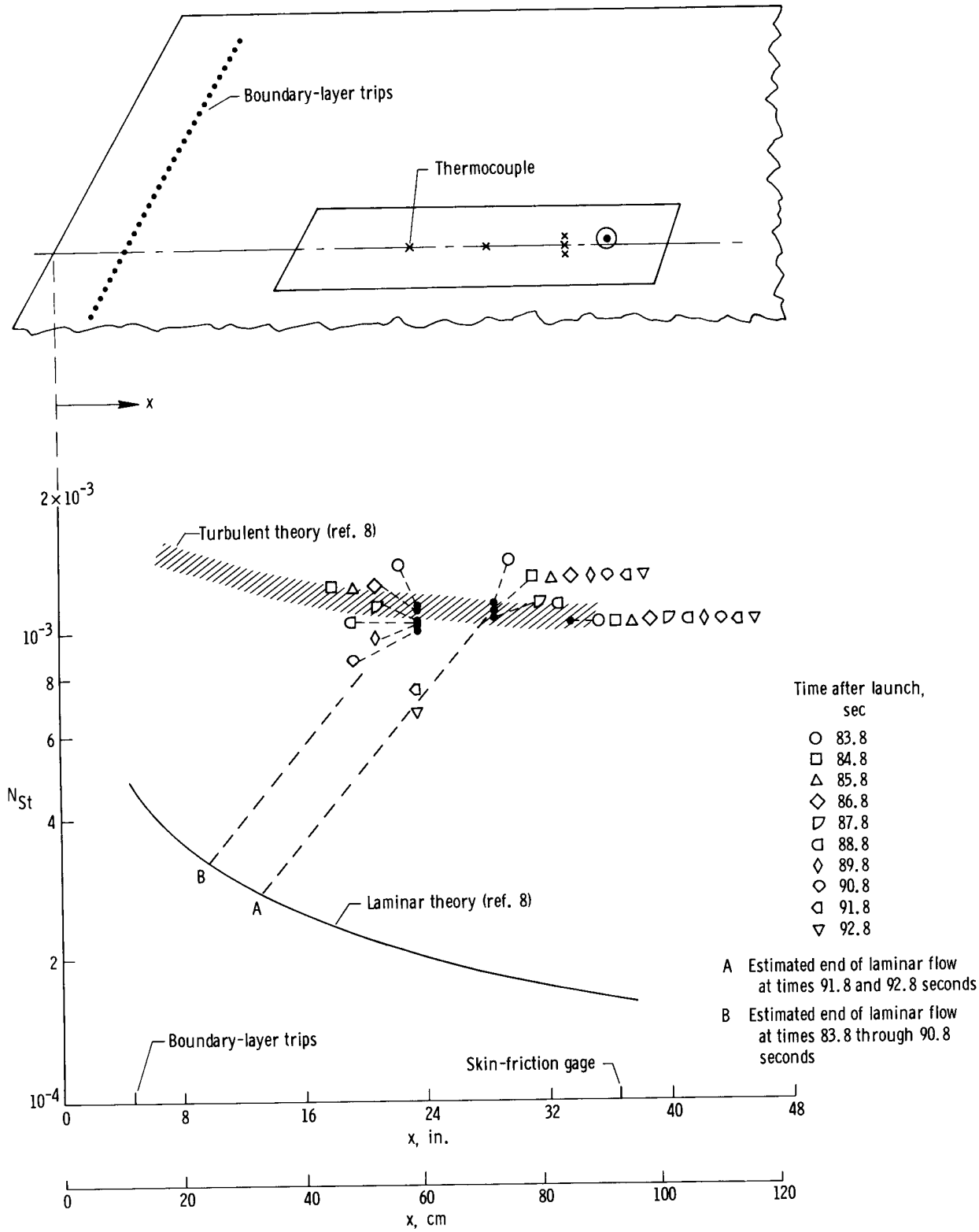

Figure 7.– Heat-transfer distribution on test panel showing estimated location of transition. $N_{Re,l}$ = 1.65 x 10^6 per ft (5.41 x 10^6 per m).

REFERENCES

1. Banner, Richard D.; Kuhl, Albert E.; and Quinn, Robert D.: Preliminary Results of Aerodynamic Heating Studies on the X-15 Airplane. NACA TM X-638, 1962.

2. Quinn, Robert D.; and Kuhl, Albert E.: Comparison of Flight-Measured and Calculated Turbulent Heat Transfer on the X-15 Airplane at Mach Numbers From 2.5 to 6.0 at Low Angles of Attack. NASA TM X-939, 1964.

3. Banas, Ronald P.: Comparison of Measured and Calculated Turbulent Heat Transfer in a Uniform and Nonuniform Flow Field on the X-15 Upper Vertical Fin at Mach Numbers of 4.2 and 5.3. NASA TM X-1136, 1965.

4. Quinn, Robert D.; and Palitz, Murray: Comparison of Measured and Calculated Turbulent Heat Transfer on the X-15 Airplane at Angles of Attack up to 19.0°. NASA TM X-1291, 1966.

5. Quinn, Robert D.; and Olinger, Frank V.: Heat-Transfer Measurements Obtained on the X-15 Airplane Including Correlation With Wind-Tunnel Results. NASA TM X-1705, 1969.

6. Banner, Richard D.; and Kuhl, Albert E.: A Summary of X-15 Heat-Transfer and Skin-Friction Measurements. NASA TM X-1210, 1966.

7. Garringer, Darwin J.; and Saltzman, Edwin J.: Flight Demonstration of a Skin-Friction Gage to a Local Mach Number of 4.9. NASA TN D-3830, 1967.

8. Eckert, Ernst R. G.: Survey of Boundary Layer Heat Transfer at High Velocities and High Temperatures. WADC Tech. Rep. 59-624, Wright Air Dev. Center, U.S. Air Force, Apr. 1960. (Available from ASTIA as AD 238292.)

9. van Driest, E. R.: The Problem of Aerodynamic Heating. Aeron. Eng. Rev., vol. 15, no. 10, Oct. 1956, pp. 26-41.

10. Bertram, Mitchel H.; Cary, Aubrey M., Jr.; and Whitehead, Allen H., Jr.: Experiments With Hypersonic Turbulent Boundary Layers on Flat Plates and Delta Wings. Hypersonic Boundary Layers and Flow Fields, AGARD Conference Proceedings No. 30, May 1968, pp. 1-1—1-21.

11. Samuels, Richard D.; Peterson, John B., Jr.; and Adcock, Jerry B.: Experimental Investigation of the Turbulent Boundary Layer at a Mach Number of 6 With Heat Transfer at High Reynolds Numbers. NASA TN D-3858, 1967.

12. Hopkins, Edward J.; Rubesin, Morris W.; Inouye, Mamoru; Keener, Earl R.; Mateer, George C.; and Polek, Thomas E.: Summary and Correlation of Skin-Friction and Heat-Transfer Data for a Hypersonic Turbulent Boundary Layer on Simple Shapes. NASA TN D-5089, 1969.

13. Bertram, Mitchel H.; and Neal, Luther, Jr.: Recent Experiments in Hypersonic Turbulent Boundary Layers. NASA paper presented at AGARD Specialists Meeting on Recent Developments in Boundary-Layer Research (Naples, Italy), May 10-14, 1965.

14. Mechtly, E. A.: The International System of Units - Physical Constants and Conversion Factors. NASA SP-7012, 1964.

15. Hansen, C. Frederick: Approximations for the Thermodynamic and Transport Properties of High-Temperature Air. NASA TR R-50, 1959. (Supersedes NACA TN 4150.)

16. Sachs, G.; and Pray, R. Ford, III, eds.: Air Weapons Materials Application Handbook Metals and Alloys. First ed., TR 59-66, USAF Air Res. and Develop. Command, Dec. 1959. (Available from ASTIA as AD 252301.)

17. Ohlsen, P. E.; and Etemad, G. A.: Spectral and Total Radiation Data of Various Aircraft Materials. Rep. No. NA 57-330, North American Aviation, Inc. (Los Angeles, Calif.), July 23, 1957.

18. Peterson, John B., Jr.: A Comparison of Experimental and Theoretical Results for the Compressible Turbulent-Boundary-Layer Skin Friction With Zero Pressure Gradient. NASA TN D-1795, 1963.

19. Spalding, D. B.; and Chi, S. W.: The Drag of a Compressible Turbulent Boundary Layer on a Smooth Flat Plate With and Without Heat Transfer. J. Fluid Mech., vol. 18, part I, Jan. 1964, pp. 117-143.

20. Westkaemper, John C.: Step-Temperature Effects on Direct Measurements of Drag. AIAA J., vol. 1, no. 7, July 1963, pp. 1708-1710.

21. Rubesin, Morris W.: A Modified Reynolds Analogy for the Compressible Turbulent Boundary Layer on a Flat Plate. NACA TN 2917, 1953.

22. von Kármán, Th.: The Analogy Between Fluid Friction and Heat Transfer. ASME Trans., vol. 61, no. 8, Nov. 1939, pp. 705-710.

23. Colburn, Allan P.: A Method of Correlating Forced Convection Heat Transfer Data and a Comparison With Fluid Friction. Trans. Amer. Inst. Chem. Eng., vol. 29, 1933, pp. 174-210.

24. Yule, G. Udny; and Kendall, M. G.: An Introduction to the Theory of Statistics. Fourteenth ed., Charles Griffin & Company Limited (London), 1958. (Available from Hafner Pub. Co., N. Y.)

25. Larson, Terry J.; and Washington, Harold P.: Summary of Rawinsonde Measurements of Temperature, Pressure Heights, and Winds Above 50,000 Feet Along a Flight-Test Range in the Southwestern United States. NASA TN D-192, 1960.

26. Meteorological Data Accuracies Committee; Meteorological Working Group; and Inter-Range Instrumentation Group: Meteorological Equipment Data Accuracies. IRIG Doc. 110-64, Mar. 1965.

27. Fieldhouse, I. B.; and Lang, J. I.: Measurement of Thermal Properties. Tech. Rep. 60-904, Wright Air Dev. Div., U.S. Air Force, July 1961.

28. Ames Research Staff: Equations, Tables, and Charts for Compressible Flow. NACA Rep. 1135, 1953. (Supersedes NACA TN 1428.)

29. Beers, Yardley: Introduction to the Theory of Error. Second ed., Addison-Wesley Pub. Co., Inc., 1962.

30. Coles, D. E.: The Turbulent Boundary Layer in a Compressible Fluid. Rep. R-403-PR, The Rand Corp., Sept. 1962.

31. Holloway, Paul F.; and Sterrett, James R.: Effect of Controlled Surface Roughness on Boundary-Layer Transition and Heat Transfer at Mach Numbers of 4.8 and 6.0. NASA TN D-2054, 1964.

32. Coles, Donald: Measurements of Turbulent Friction on a Smooth Flat Plate in Supersonic Flow. J. Aeron. Sci., vol. 21, no. 7, July 1954, pp. 433-448.

TABLE I. – FLIGHT PARAMETERS

t,[a] sec	M_∞	p_∞		T_∞		$N_{Re,\infty}$		$\delta_{v,eff}$, deg
		lb/ft^2	hN/m^2	°R	°K	per ft	per m	
83.8	5.19	62	29.7	405	225	1.57×10^6	5.15×10^6	0.7
84.8	5.20	61	29.2	405	225	1.55	5.09	.7
85.8	5.22	61	29.2	405	225	1.56	5.12	.7
86.8	5.24	61	29.2	405	225	1.56	5.12	.7
87.8	5.25	60	28.7	405	225	1.54	5.05	.7
88.8	5.27	59	28.2	406	226	1.54	5.05	.7
89.8	5.30	59	28.2	406	226	1.54	5.05	.7
90.8	5.33	59	28.2	406	226	1.54	5.05	.7
91.8	5.33	59	28.2	406	226	1.54	5.05	.7
92.8	5.33	58	27.8	406	226	1.51	4.95	.7

[a]Times after launch at which heat-transfer and skin-friction coefficients were derived.

Note: Jettisonable shield was released 82.6 seconds after launch.

TABLE II. – MEASURED WALL TEMPERATURES, SHEARING STRESSES, HEAT-TRANSFER COEFFICIENTS, SURFACE STATIC PRESSURES, AND CALCULATED LOCAL FLOW PARAMETERS

t, sec	$\frac{T_w}{T_R}$	T_w		τ		h_H		$p_{l,av}$		V_l		$\rho_l V_l$		$N_{Re,k}$
		°R	°K	lb/ft^2	hN/m^2	lbm/ft^2 sec	kg/m^2 sec	lb/ft^2	hN/m^2	ft/sec	m/sec	lbm/ft^2 sec	kg/m^2 sec	
83.8	0.218	485	270	2.30	1.10	2.06×10^{-2}	10.05×10^{-2}	101	48.4	5004	1525	19.10	93.20	4.13×10^{6}
84.8	.233	520	289	2.30	1.10	2.04	9.96	101	48.4	5018	1529	19.16	93.50	4.13
85.8	.246	554	308	2.30	1.10	2.05	10.00	101	48.4	5035	1535	19.24	93.89	4.16
86.8	.260	590	328	2.30	1.10	2.06	10.05	101	48.4	5052	1540	19.25	93.94	4.16
87.8	.273	619	344	2.30	1.10	2.04	9.96	101	48.4	5062	1543	19.29	94.14	4.16
88.8	.285	652	363	2.30	1.10	2.04	9.96	101	48.4	5089	1551	19.29	94.14	4.16
89.8	.295	681	379	2.30	1.10	2.06	10.05	101	48.4	5116	1559	19.34	94.38	4.16
90.8	.307	713	396	2.30	1.10	2.06	10.05	101	48.4	5145	1568	19.40	94.70	4.16
91.8	.320	743	413	2.30	1.10	2.07	10.10	101	48.4	5145	1568	19.40	94.70	4.16
92.8	.333	776	431	2.30	1.10	2.09	10.20	101	48.4	5145	1568	19.40	94.70	4.16